Ceramics International 44 (2018) 22329–22338

Contents lists available at ScienceDirect

Ceramics International

journal homepage: www.elsevier.com/locate/ceramint

Stabilized β-Bi_2O_3 nanoparticles from $(BiO)_4CO_3(OH)_2$ precursor and their photocatalytic properties under blue light

Karen Valencia G.[a], Alejandro López[a], Agileo Hernández-Gordillo[a,*,1], Rodolfo Zanella[b], Sandra E. Rodil[a]

[a] Instituto de investigaciones en Materiales, Universidad Nacional Autónoma de México, Circuito Exterior SN, Ciudad Universitaria, CP 04510 Mexico City, Coyoacán, Mexico

[b] Instituto de Ciencias Aplicadas y Tecnología, Universidad Nacional Autónoma de México, Circuito Exterior SN, Ciudad Universitaria, CP 04510 Mexico City, Coyoacán, Mexico

ARTICLE INFO

Keywords:
Stabilization
Pure β-Bi_2O_3
Amorphous precursor
Blue-photodegradation

ABSTRACT

Stabilized tetragonal Bi_2O_3 nanoparticles (β-Bi_2O_3) were obtained by annealing treatments of amorphous Bi-based precursors, obtained by chemical precipitations, at temperatures between 350 and 450 °C. The formation of the stabilized β-Bi_2O_3 phase was possible by using $(BiO)_4CO_3(OH)_2$ while other precursors such as amorphous bismuth carbonate ($(BiO)_2CO_3$) and amorphous basic bismuth nitrate ($Bi_6O_6(OH)_2(NO_3)_4{\cdot}2H_2O$) led to the formation of the thermodynamically stable monoclinic α-Bi_2O_3 and $Bi_5O_7NO_3$ phases. The Bi-based precursors were prepared by the chemical precipitation method at room temperature in ethylenediamine-solvent varying the HNO_3/Bi^{3+} molar ratio (10, 26 and 56). The physicochemical properties of the three as-prepared amorphous precursors and the formed-after-calcination β-Bi_2O_3, α-Bi_2O_3 and $Bi_5O_7NO_3$ phases were analyzed by X-ray diffraction, scanning electron microscopy, thermogravimetry, X-ray photoelectron spectroscopy (XPS), FTIR analysis, diffuse reflectance spectroscopy and surface area by BET method. The photocatalytic activity of all annealed solids containing the β-Bi_2O_3 phase was tested in the photodegradation of the indigo carmine (IC) dye under specific blue light. A schematic diagram of the Bi_2O_3 phases obtained as a function of the annealing conditions and initial amorphous precursor is proposed and explained in terms of the amount of CO_3^{2-}, NO_3^- and amine ($ENH_2^{2+} \Leftrightarrow ENH^+$) ions present in each bismuth precursor.

1. Introduction

Bi_2O_3 possesses six different polymorphous phases: α-Bi_2O_3 (monoclinic), β-Bi_2O_3 (tetragonal), γ-Bi_2O_3 (FCC), δ-Bi_2O_3 (cubic), ε-Bi_2O_3 (triclinic) and ω-Bi_2O_3 (triclinic) [1], where α and δ are thermodynamically stable phases at low and high temperature, respectively, while the others are metastable. The optical band gap of Bi_2O_3 varies from 2.0 to 3.9 eV, depending of the crystalline phase [2], making this material suitable for various applications such as in optoelectronics [3], electrochemical capacitors [4,5], gas sensors [6] and as catalysts/photocatalysts [7–15]. For many of these applications, it is crucial to obtain pure phase materials or well-defined fractions of mixed phases, which is not always achieved [8,16–18]. For visible-light photocatalysis, the metastable β-Bi_2O_3 phase is attractive due to the small band gap (2.4 eV), however, it is more difficult to obtain than the α-Bi_2O_3 phase, which is the most stable one at room temperature [19–25], notwithstanding, its band gap (2.9 eV) limits its light-adsorption capacity in the visible region. The metastable β-Bi_2O_3 phase can be well activated in visible light, but just a few works have been devoted to the production of β-Bi_2O_3 because it is difficult to stabilize in a wide temperature interval [26–29]. Nonetheless, β-Bi_2O_3 has shown higher photocatalytic activity than the α-Bi_2O_3 phase [29–32], and for this reason the pure β-Bi_2O_3 phase is still of great significance.

Different strategies have been successfully used to obtain an adequate bismuth precursor to be transformed into the metastable β-Bi_2O_3 phase by calcination processes [33]. Commonly, the bismuth precursor is obtained by a hydrothermal method at 160–180 °C, where bismuth trinitrate pentahydrate [$Bi(NO_3)_3{\cdot}5H_2O$] is commonly diluted in an aqueous solution of nitric acid (HNO_3), adding an additive that can be Na_2CO_3 [32,34,35], NH_4HCO_3 [36], L-lysine-oxalic [37] or citric acid [33,38], all of them in NaOH presence, obtaining bismuth carbonate $(BiO)_2CO_3$ with different morphologies (worm-like, flakes, flower-like)

* Corresponding author.
E-mail address: agileohg@iim.unam.mx (A. Hernández-Gordillo).
[1] CONACYT Research Fellow.

https://doi.org/10.1016/j.ceramint.2018.08.358
Received 9 April 2018; Received in revised form 29 August 2018; Accepted 31 August 2018
Available online 01 September 2018

as the main precursor to produce the β-Bi_2O_3 phase.

In contrast, by using a solvothermal method under similar thermal conditions (100–180 °C), [$Bi(NO_3)_3{\cdot}5H_2O$] is diluted in an organic solvent or mixture of them: ethylenglycol or methoxyethanol [8], dimethyl formamide (DMF) [5], acetic acid-ethanol-DMF [29], glycerol-ethanol [2] or acetic acid-ethanol [39], in absence of both HNO_3 and NaOH, obtaining in these cases amorphous precursors with different morphologies (irregular spherical, hollow spheres, hunk-like, nanosheets, etc.). This amorphous precursor has been associated with the possible formation of an intermediate $(BiO)_4(OH)_2CO_3$, which can be dehydrated/transformed into $(BiO)_2CO_3$ by annealing at 200 °C [8,40]. When the $(BiO)_2CO_3$ precursor is annealed at around 290 and 380 °C, either the pure β-Bi_2O_3 phase or mixture of the $(BiO)_2CO_3$/β-Bi_2O_3 phase is obtained [16] whereas at temperatures above 350 °C, the β-Bi_2O_3 phase starts to be transformed into the α-Bi_2O_3 phase, obtaining a mixture of both phases [38]. On the contrary, when the amorphous precursor is annealed at a similar temperature interval (270–350 °C), the pure β-Bi_2O_3 phase is formed, even the transformation toward the α-Bi_2O_3 phase occurs above 420 °C [29], indicating that the β-Bi_2O_3 phase is more stable.

In most of these works, it has been stated that the presence of carbonate (CO_3^-) ions is the key factor to obtain the β-Bi_2O_3 phase because surface-coordinated CO_3^- ions on the Bi_2O_3 surface can lower the surface energy of the β-Bi_2O_3 phase, making it stable at room temperature [1]. By contrast, the β-Bi_2O_3 phase can be returned to the bismuth oxycarbonate precursor when exposed to the environmental atmosphere or to CO_2 in solution [40].

Until now, the influence of the HNO_3 and diamine-solvent on the properties of the as-precursors to obtain the β-Bi_2O_3 phase by calcination has not been studied. Therefore, in this work, a simple chemical precipitation method to produce amorphous precursors using ethylendiamine (ENH^+) as precipitating and morphological agent (60 vol%) is proposed. The influence of the HNO_3/Bi^{3+} molar ratio (10, 26 and 56) on the preparation of three amorphous precursors and their annealing temperature (350, 400 and 450 °C) was investigated. A schematic diagram of the phases compositions obtained as functions of the annealing conditions and the initial amorphous precursor is proposed. The adsorption capacity and the photocatalytic activity properties of pure β-Bi_2O_3 and solids containing the β-Bi_2O_3 phase were explored in the photodegradation of the indigo carmine (IC) dye.

2. Experimental details

2.1. Synthesis of the amorphous precursor and Bi_2O_3

Three different as-prepared solids were obtained by the chemical precipitation method, where the Bi^{3+} concentration in aqueous solution was fixed at 41 mM and the concentration of nitric acid (HNO_3) was varied (0.6, 1.5 and 3.5 M), leading to a HNO_3/Bi^{3+} molar ratio = 10, 26 and 56, respectively. A homogeneous solution of Bi $(NO_3)_3{\cdot}5H_2O$ (Aldrich) was prepared by adding the appropriate amount of nitric acid (HNO_3, Baker Analyzed) under constant stirring until getting a stable transparent bismuth solution. Afterwards, 60 vol% of ethylenediamine-solvent (ENH^+, Aldrich) was added dropwise into the bismuth acid solution under cold water bath (room temperature), leaving the suspension under vigorous magnetic stirring for 2 h. The resulting precipitate was collected by filtration, washing with an ethanol-water solution and left to dry at room temperature. The as-prepared solids were labeled as **NBX**, where **NB** represents the [HNO_3/Bi^{3+}] molar ratio and X represents the ratio value (10, 26 and 56). Each solid was annealed at three temperatures (350, 400 and 450 °C) in static air for 2 h, using a heating rate of 10 °C/min. The materials were labeled as **NBX-Z**, where **Z** represents the annealing temperature.

2.2. Characterization of Bi_2O_3

The as-prepared solids and the annealed Bi_2O_3 materials were characterized by powder X-ray diffraction (XRD) using a Siemens D500 diffractometer with Cu Kα radiation of 0.15406 nm (34 kV, 25 mA) and scanning range between 15 and 60 °C (2 theta) with a step size of 0.013°/s. For the lattice parameter determination, the Bragg law was used considering the corresponding structure for each phase. The phase composition and average crystal size were obtained by using the Halder-Wagner method in the PDXL2 software.

The FTIR absorption spectra of all the samples were recorded on a Thermoscientific Nicolet 6700 spectrometer using an attenuated total reflection (ATR) accessory equipped with a diamond crystal; for each measurement, the powder was placed and the pressure was of 815 Psi at room temperature. Typically, 68 scans at a resolution of 4 cm^{-1} in the interval ranging from 600 and 4000 cm^{-1} in the transmittance mode were used.

The chemical composition of the as-prepared and annealed solids were evaluated by X-ray photoelectron spectroscopy (XPS) using the XPS microprobe PHI 5000 Versa Probe II of Physical Electronics. A monochromated Al K_α ($h\nu$ = 1486.6 eV) X-ray source was used at 25 W with 100 μm of beam diameter. The surface of each sample was etched for 5 min with 1 kV Ar+ at 500 nA current. The XPS spectra were acquired at 45° from the surface in a constant pass energy mode (CAE) at E_0 = 117.40 and 11.75 eV for survey and high-resolution spectra, respectively. The adventitous C1s signal at 284.8 eV was used to correct the binding energies.

Thermal analysis (TGA) of the samples was performed up to 800 °C at a heating rate of 10 °C/min in static air atmosphere using a TA Instruments SDT Q600 V8.3 Build 101. The Bi_2O_3 morphology was revealed by scanning electron microscopy (SEM) using a JEOL 7600F operated at 10 kV. The UV–vis diffuse reflectance spectra (DRS) were accomplished on a UV–vis spectrophotometer (Shimadzu 2600) equipped with an integration sphere (ISR 2600) in the interval ranging from 200 to 700 nm and using $BaSO_4$ as a reference blank. The spectra were converted from reflectance to absorbance by the Kubelka-Munk method. The band gap energy (E_g) was calculated by extrapolating the linear portion of the $(F(R) \times h\nu)^2$ versus $h\nu$ curves to F(R) = 0 [41], considering its corresponding allowed transition for each phase composition (see Table 1).

The specific surface area of the semiconductors was determined by the BET method from the nitrogen adsorption-desorption isotherms at −196 °C using a Quantachrome Autosorb-1 automatic instrument. Prior to the adsorption procedure, the samples were out-gassed under

Table 1
Sample name, phase composition, allowed transition type and band gap energies value for all prepared solids.

Sample	Phases composition	Allowed transition	Band gap (eV)	[a]Sg (m^2/g)
NB10	Amorphous	UNKNOWN	3.52	
350 °C	α / β-Bi_2O_3	DIRECT	2.43	~ 4
400 °C	β / α-Bi_2O_3	DIRECT	2.86	–
450 °C	α-Bi_2O_3	DIRECT	2.86	–
NB26	Amorphous-$(BiO)_4CO_3(OH)_2$	INDIRECT	3.63	–
350-400 °C	β-Bi_2O_3	DIRECT	2.42	–
450 °C	α / β-Bi_2O_3	DIRECT	2.42	~ 5
NB56	Amorphous-$Bi_6O_6(OH)_2(NO_3)_4{\cdot}2H_2O$	INDIRECT	3.37	–
350 °C	$(BiO)_2CO_3$ / β-Bi_2O_3	DIRECT or INDIRECT/ DIRECT	2.40	~ 8
400-450 °C	$(BiO)_2CO_3$/β-Bi_2O_3/ $Bi_5O_7NO_3$	DIRECT INDIRECT/ DIRECT	2.40	–

[a] Sg = Specific Surface Area.

high vacuum at 150 °C for 6 h. The Brunauer-Emmett-Teller method (BET method) was applied to calculate the specific surface area.

2.3. Photocatalytic tests under blue light

The photodegradation reaction was performed in an open air-glass-photoreactor system containing 200 mL of an aqueous solution at 5 ppm of *indigo carmine* (*IC*) dye and 20 mg of photocatalyst powder, leading to a load of 0.1 g/L. The suspension was maintained under magnetic stirring at 1000 RPM, room temperature and without any pH adjustment (natural pH = 7). The system was irradiated by means of a blue LED-lamp of 10 W (maximum emitting light at λ = 450 nm) placed at the top of the suspension (at 3 cm of distance). Before irradiation, the suspension was kept under dark conditions for 40 min to ensure the adsorption-desorption equilibrium. The estimation of the *IC* dye concentration was done by taking a filtered aliquot of 3 mL at time intervals for 50 min, and analyzing the aliquot absorbance (absorption band at 610 nm for *IC* dye) using UV–vis spectroscopy on a Shimadzu 1800 spectrometer. The reaction kinetics was carried out considering the Langmuir Hinshelwood kinetic model. At low adsorption or reactant concentration, the reduction rate (r) can be simplified to pseudo first order kinetics with an apparent rate constant (k_{app}), where the reactant concentration after reaching equilibrium was taken as the initial concentration (C_0), which is expressed as follows: $\ln\left(\frac{C}{C_0}\right) = -k_r k_{ads} C = -k_{app} t$, where k_r is the rate constant and k_{ads} is the adsorption equilibrium constant. Plotting $\ln\left(\frac{C}{C_0}\right)$ versus reaction time (t) yields a straight line, and the slope is the apparent kinetic rate constant (k_{app}).

3. Results and discussion

3.1. Crystalline structure and phase composition

The crystalline phases of the as-prepared solids at different HNO_3/Bi^{3+} molar ratios and the solids annealed at 350–450 °C were obtained by XRD. The patterns of all the annealed solids from the as-prepared sample at HNO_3/Bi^{3+} molar ratio of 10 are shown in Fig. 1A. The as-prepared solid (**NB10**) exhibited a wide peak at around ~ 28° in 2θ, suggesting that it is an amorphous-like compound, however, until now, it has not been identified. An amorphous product has been similarly obtained when $BiONO_3$ reacts with a weak-alkaline amine like NH_4OH or hexamethylenetetramine (HMT-solvent), depending on its concentration, and has been used as a precursor of Bi_2O_3 solids [8]. When annealed at 350 °C (**NB10–350**) exhibits diffraction peaks at 28.08°, 31.73°, 32.98°, 46.30°, 47.12° and 55.75° in 2θ, which are mainly indexed to β-Bi_2O_3 phases (JCPDS card no. 01-076-0147), however, two reflection peaks at 27.41° and 33.38° in 2θ suggest the presence of the α-Bi_2O_3 phase (JCPDS card no. 01-071-2274). By applying the Halder-Wagner method in the PDXL2 software, the phase composition of the **NB10–350** sample was found to be mainly represented by 70% of the β-Bi_2O_3 phase. When the amorphous product is annealed at 400 °C (**NB10–400**), it exhibits diffracted peaks at 2θ = 25.83°, 26.90°, 27.41°, 28.11°, 33.35° and 46.40° of the principal planes (002), (-112), (-121) (012), (-202-200) and (041) corresponding to the α-Bi_2O_3 phase, but small peaks related to the β-Bi_2O_3 phase can be also detected, representing ~ 11% of the β-Bi_2O_3 phase. At 450 °C, the **NB10–450** solid is mainly composed of the well-crystallized α-Bi_2O_3 phase. By applying the Halder-Wagner method, the grain size of the α-Bi_2O_3 phase falls within the interval ranging from 14 to 20 nm. The grain size for the β-Bi_2O_3 phase in the **NB10–350** solid is 21 nm. These results are in good agreement with what has been reported in the literature, where compounds like $(H_2O)_{0.75}Bi_2(CH_3COO)(NO_3)_{1.12}$ or $(BiO)_2CO_3$ have been used as bismuth precursors to obtain the β-Bi_2O_3 phase, being immediately transformed into the stable α-Bi_2O_3 phase at temperatures above 350 °C [16,29].

The XRD patterns of the as-prepared sample at HNO_3/Bi^{3+} molar ratio = 26 and those of the annealed solids are shown in Fig. 1B. The **NB26** solid exhibits small wide peaks at around 27.36°, 32.89–33.45° and 47.50° in 2θ, suggesting the presence of an amorphous product (not identified). Additionally, it exhibits a peak at a low angle of ~ 7° in 2θ, which suggests a lamellar structure [42]. The amorphous product annealed at 350, 400 and 450 °C exhibits main diffracted peaks at 2θ = 28.01°, 31.74°, 32.78°, 46.21°, 47.04°, 54.27°, 55.52° and 57.75°, which are associated with the (201), (002), (220), (400), (302), (213), (421), (402) planes that are indexed to the tetragonal-β-Bi_2O_3 phase (JCPDS card no. 01-078-1793), however, at 450 °C, a small peak (at 25.82°) related to the α-Bi_2O_3 phase (18%) is detected, indicating that at this temperature starts its transformation. In comparison to the annealed **NB10** sample (Fig. 1A), the β-Bi_2O_3 phase is well stabilized even at 450 °C, which was unexpected because β-Bi_2O_3 has been stabilized at temperatures below 420 °C from an amorphous product prepared in organic solvent [29,39]. In our case, the amorphous product precipitated in aqueous solution in the presence of appropriate amounts of HNO_3/Bi^{3+} (26), which is adequate to produce well-stabilized β-Bi_2O_3 and it could extend its applicability to other catalytic processes. By applying the Halder-Wagner method, the grain size (crystalline domain) of the tetragonal phase was increased from 16 to 44 nm.

By increasing the HNO_3/Bi^{3+} molar ratio to 56, the as-prepared sample (**NB56**) exhibits small wide peaks centered at around ~ 11°, 28.1–28.7° and 29.7° in 2θ, suggesting an amorphous-nanocrystalline-like compound (see Fig. 1C), however, the defined peaks could be related to the possible formation of basic bismuth nitrate ($Bi_6O_6(OH)_2(NO_3)_4{\cdot}2H_2O$) (Card. No. 28-0654). This intermediate precursor has been similarly obtained in 2-methoxyethanol in the presence of an amine solvent (hexamethylenetetramine) at pH from 2.5 to 6

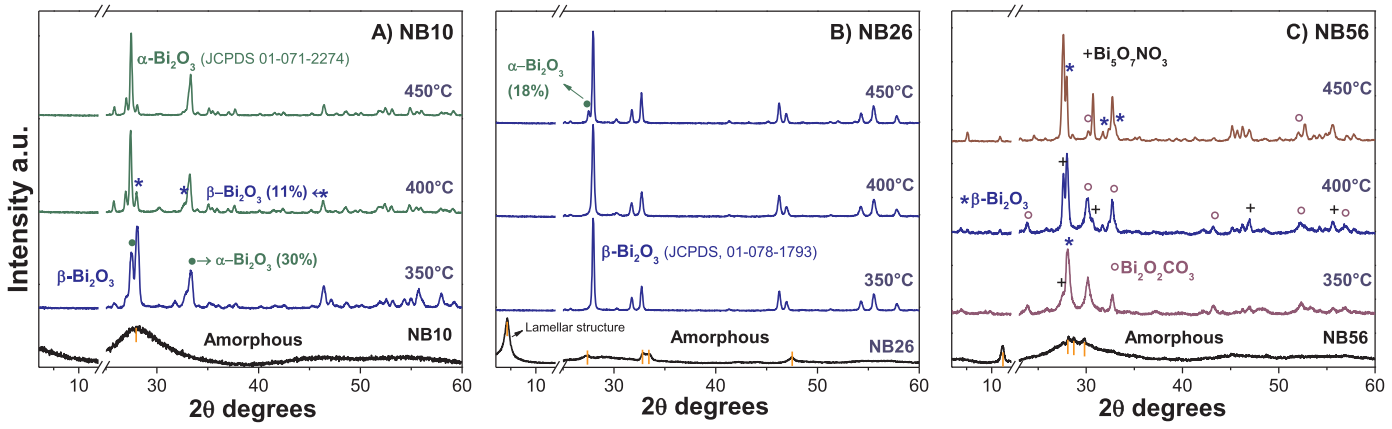

Fig. 1. XRD patterns of the solids annealed from 350 to 450 °C and the as-prepared samples at different molar ratio HNO_3/Bi^{3+}; A) 10, B) 26 and C) 56.

[8,43,44]. When the solid is annealed at 350 °C (**NB56–350),** it exhibits diffraction peaks at 28.07°, 30.11°, 32.74°, 43.16°, 52.35° and 56.8° in 2θ, which identifies it as $(BiO)_2CO_3$ (JCPDS 01-084-1752) with 93% of contribution. In addition, the reflection peak at 28.01° is associated with the β-Bi_2O_3 phase and the small peak at 27.56° is related in minor proportion to $Bi_5O_7NO_3$ (card. 00-051-0525). After the calcination at 400 and 450 °C, diffracted peaks of the $(BiO)_2CO_3$, β-Bi_2O_3 and $Bi_5O_7NO_3$ phases are still present at different proportions, however, the contribution of the $Bi_5O_7NO_3$ phase was increased whereas that of $(BiO)_2CO_3$ was decreased as the temperature was increased. So, a mixture of β-Bi_2O_3 and $Bi_5O_7NO_3$ was mainly detected, where by applying the Halder-Wagner method in the PDXL2 software, the contribution of each one is 49% and 51%, respectively. This means that nanocrystalline $Bi_6O_6(OH)_2(NO_3)_4{\cdot}2H_2O$ is formed in aqueous solution at high nitric acid concentration, and it is gradually transformed without the formation of the α-Bi_2O_3 phase as follows: $(BiO)_2CO_3$ → β-Bi_2O_3 → $Bi_5O_7NO_3$.

3.2. FT-IR analysis

FTIR spectra of the as-prepared samples and the solids annealed at 350–450 °C are shown in Fig. 2A–C. For the amorphous product **NB10** (Fig. 2A), it displays signals at 815 and 1038 cm^{-1}, which are characteristic of mono-dentate and stretching vibrations of the NO_3^- group, respectively. These signals must be accompanied by a broad signal at 1274–1300 cm^{-1} of asymmetric stretching modes of the NO_3^- group [45,46], however, it appears to be overlapped with a broad band at 1319 cm^{-1}. In addition, the signal at 3270 cm^{-1} is related to the stretching vibrations of OH^- groups, suggesting the presence of some type of basic bismuth nitrate $[Bi_6O_4(OH)_4(NO_3)_6\ 7H_2O$, $Bi_6O_5(OH)_3(NO_3)_5\ 3H_2O$, $Bi_6O_6(OH)_2(NO_3)_4\ 1.5H_2O$ [46,47], which are not well crystallized. The signal at 1319 cm^{-1} is assigned to stretching vibrations of C-N groups [48] and it can be originated from the diamine-solvent (ENH^+-solvent), suggesting that it is present in the material structure. On the other hand, the signal at 843 cm^{-1} is characteristic of the out-of-plane bending mode of free CO_3^{2-} (ν_2), characteristic of $(BiO)_2CO_3$ [49], however, the symmetric stretching mode ν_1 at 1067 cm^{-1} and the anti-symmetric vibration ν_3 at 1470 and 1390 cm^{-1} are not seen [50–52], because they are overlapped with the signal at 1429 cm^{-1}, which is not identified. The signal at 1540 cm^{-1} is assigned to deformation vibrations of hydroxyl groups and molecular water, which can be generated from carbonate compounds containing OH^- groups like $(BiO)_4CO_3(OH)_2$. This compound has been reported as an amorphous carbonate intermediate due to its incomplete transformation into $(BiO)_2CO_3$ [53,54]. When the amorphous solid was annealed at 350 °C, the vibration signals of NO_3^-, C-N and OH^- groups are absent, suggesting that basic bismuth nitrate, ethylenediamine and $(BiO)_4CO_3(OH)_2$ were decomposed. However, the vibration signals characteristic of free CO_3^{2-} (ν_2, 1380 and 1470 cm^{-1}) were observed, even remaining at 450 °C, indicating the presence of small proportions of $(BiO)_2CO_3$. This fact means than the amorphous carbonate intermediate, $(BiO)_4CO_3(OH)_2$, was dehydrated/transformed into the $(BiO)_2CO_3$ precursor while β-Bi_2O_3 was transformed into α-Bi_2O_3.

For the amorphous **NB26** solid (Fig. 2B), in addition to the bands of vibrational modes of the CO_3^{2-} group (848, 1013, 1388 cm^{-1}), stretching and bending modes of the OH^- group (3326, 1538 cm^{-1}) can be seen [49,55]. All these vibration signals are characteristic of $(BiO)_4CO_3(OH)_2$ compounds, suggesting that the amorphous carbonate intermediate was well formed. The high intensity of these bands suggests that amorphous $(BiO)_4CO_3(OH)_2$ compounds are more favored by increasing the HNO_3 content. The signal at 1336 cm^{-1}, assigned to the stretching vibrations of C-N groups [48], is also observed, suggesting the presence of the ENH^+-molecule. After calcination at 350 °C, the β-Bi_2O_3 sample displays vibration signals corresponding to $(BiO)_2CO_3$ (848, 1388, 1465 cm^{-1}), which decreases its contents as the calcination temperature is increased. It has been reported that the presence of CO_3^{2-} groups in the β-Bi_2O_3 phase matrix could help stabilize its structure at temperatures close to 380 °C [1]. Nevertheless, in our case, at a calcination temperature of 450 °C, the vibration signals of $(BiO)_2CO_3$ are almost absent, and the β-Bi_2O_3 phase continues being stable (seen Fig. 1B). The presence of $(BiO)_4CO_3(OH)_2$ compounds could be the responsible for inducing the stabilization of the pure β-Bi_2O_3 phase.

By increasing the HNO_3/Bi^{3+} molar ratio to 56, the basic bismuth nitrate solid (Fig. 2C) shows the vibrational bands (815, 843 and 1036 cm^{-1}) of the NO_3^- groups [45] and vibrational bands (1623, 3419 cm^{-1}) of the OH^- superficial groups of adsorbed water [47]. In addition, it also displays the vibrational modes of the C–N bond (1330 cm^{-1}) associated with the ENH^+-molecule. This fact confirms that the nanocrystalline solid is composed of a type of basic bismuth nitrate. According to the XRD analysis (Fig. 1C), all these vibration signals are generated by the $Bi_6O_6(OH)_2(NO_3)_4{\cdot}2H_2O$ compound [45], which is dehydroxylated during the calcination at 350–450 °C, forming the $Bi_5O_7NO_3$ compound. Vibration signals of the $(BiO)_2CO_3$ compound are also exhibited, as it can be seen in the XRD patterns mentioned above (Fig. 1C). The vibration signal of the ENH^+-molecule (1330 cm^{-1}) is also present, which also appears at 400 °C, indicating that it was hard to be eliminated. The bands at 815, 1036, 1295 and 1373 cm^{-1}, assigned to $Bi_5O_7NO_3$, [45] are more intense as the calcination temperature increases, whereas the CO_3^{2-} and C-N signals decrease, indicating that the ENH^+-molecule and $(BiO)_2CO_3$ were decomposed. This fact means that at high HNO_3 contents and in the presence of an diamine-solvent, basic bismuth nitrate ($Bi_6O_6(OH)_2(NO_3)_4{\cdot}2H_2O$) is preferably formed and it continues to be transformed into $Bi_5O_7NO_3$ during the calcination process.

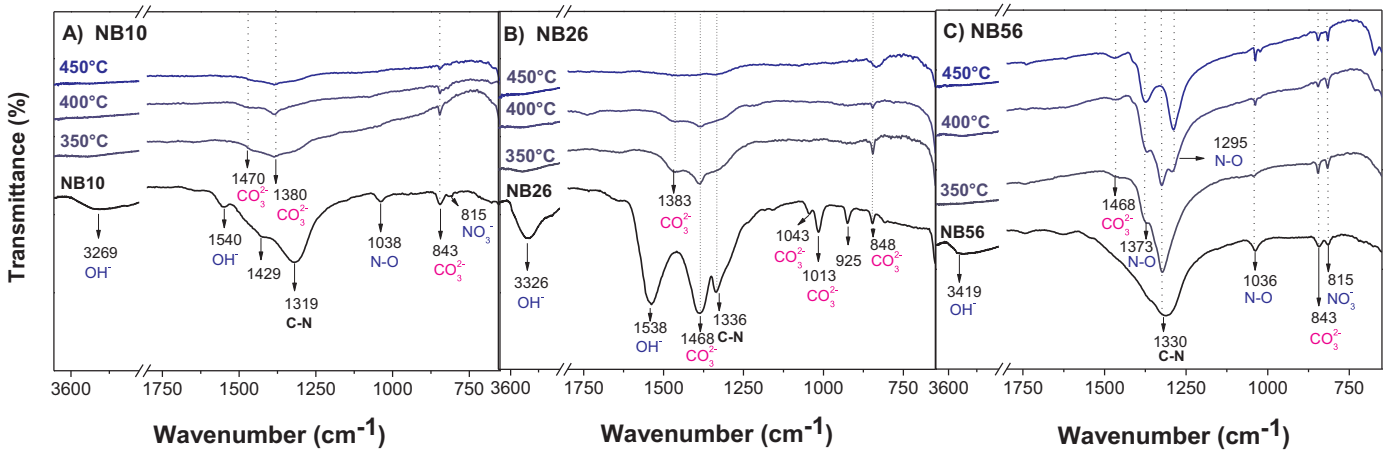

Fig. 2. FTIR analysis for the as-prepared samples at molar ratio HNO_3/Bi^{3+}; A) 10, B) 26 and C) 56, and of the annealed solids from 350 to 450 °C.

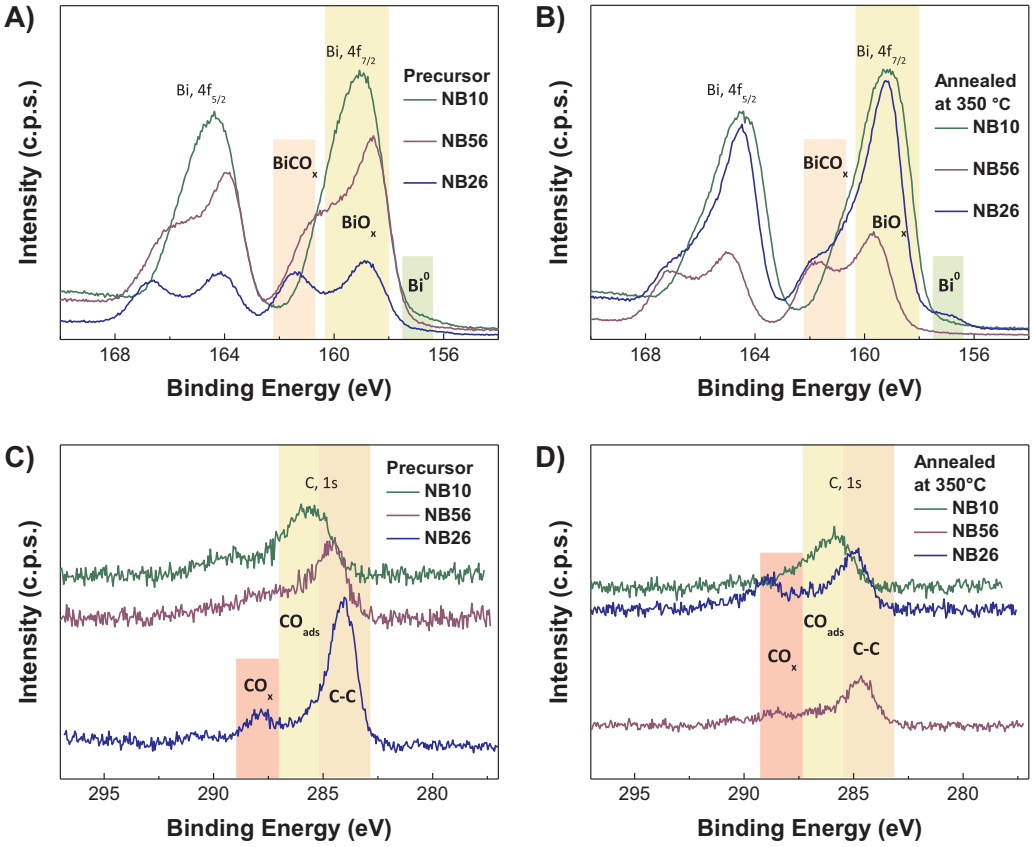

Fig. 3. XPS spectra of Bi*4f* and C*1s* for: A, C) as-prepared solids at different molar ratio HNO_3/Bi^{3+} and B, D) annealed solids at 350 °C.

3.3. XPS analysis

X-ray photoelectron spectroscopy (XPS) measurements of as-prepared and annealed solids were carried out to investigate the variations in the surface chemical composition as a consequence of the different molar ratio of HNO_3/Bi^{3+} used for its preparation. Fig. 3A shows the high resolution XPS spectra of Bi*4f* photoelectron signal for the as-prepared solids at different molar ratio (HNO_3/Bi^{3+}). For the amorphous **NB10** solid, the spectra show the two spin-orbit Bi $4f_{7/2}$ and $4f_{5/2}$ doublet placed at 159.0 and 164.5 eV, suggesting the existence of Bi^{3+} that can be ascribed to Bi-O bonds of Bi_2O_3. However, these value are different to those obtained for pure Bi_2O_3 but it has been attributed to the formation of an interfacial structure and the changing in the local environment and electron density of the elements [38]. The doublet separation of energy is 5.4 eV which is in accordance to the reported in the literature for Bi^{3+} [8]. For the amorphous **NB26** solid, the spectra show two doublet peaks placed at (158.8 and 164.16 eV) and (161.4 and 166.6 eV). The first ones are assigned to Bi^{3+} ascribed to Bi_2O_3 and the second one, which is shifted at higher binding energy, suggest the presence of BiO linked to carbonate (CO_3^{2-}) ions [37,53], attributed to the presence of the carbonate intermediate compounds in concordance with the FTIR results. The amorphous **NB56** solid also exhibited peaks assigned to Bi^{3+} of Bi_2O_3 (158.6 and 164.0 eV) and clear shoulders located at slightly lower binding energies (BE) than the carbonate peaks (160.4 and 165.5 eV), which could be assigned to Bi^{3+} of the basic bismuth nitrate [45,46], in compliance with the XRD and FTIR results.

After the annealing, the spectra followed similar trends than the precursors. Fig. 3B shows the high resolution XPS spectra of the Bi*4f* signal for the annealed oxide solid at 350 °C. For the three samples, the spectra show the peaks attributed to the Bi^{3+} of Bi_2O_3, although slightly shifted to higher BE for the **NB56–350** solid and broader for the **NB10–350,** suggesting that Bi_2O_3 stoichiometry is not perfectly distributed. For the annealed **NB26** and **NB56** samples, the carbonate associate peaks at (161.4 and 166.6 eV) are clearly observed, suggesting that the carbonate compounds are still persistent as impurities, as was confirmed by XRD.

For all the solids, a small peak indicated at 156.9 eV is related to $4f_{7/2}$ Bi^0 metallic state. This is probably a consequence of a slight reduction of Bi^{3+} occurring during the Ar cleaning [56]. The chemical shift detected between Bi^0 and Bi^{3+} (2.0 eV) are in accordance to those reported in the literature [57].

Fig. 3C–D shows the high resolution XPS spectra of the C1s for the as-prepared precursor and annealed solids. For the **NB26** precursor, annealed **NB26–350** and **NB56–350** solids, a clear signal at higher BE is assigned to the carbonate ion of the bismuth carbonate [53], confirming the formation of the carbonate compounds in these sample. The peaks placed at 284.8, 286 eV are ascribed to adventitious carbon species [51].

Based on the obtained result, a schematic phase composition diagram of the type of bismuth compounds obtained from the different amorphous precursors prepared in aqueous solution at different HNO_3/Bi^{3+} molar ratios is shown in Fig. 4. When the amorphous precursor is prepared at a HNO_3/Bi^{3+} molar ratio = 10, BiOx compounds are obtained as amorphous products, giving a mixture of α/β-Bi_2O_3 phases in different proportions after calcination whereas the pure, well-stabilized β-Bi_2O_3 phase can be obtained from the amorphous $(BiO)_4CO_3(OH)_2$ compound, prepared at a HNO_3/Bi^{3+} molar ratio of 26. By increasing the HNO_3/Bi^{3+} molar ratio to 56, nanocrystalline basic bismuth nitrate ($Bi_6O_6(OH)_2(NO_3)_4{\cdot}2H_2O$) is formed, which is transformed into a mixture of $(BiO)_2CO_3$ / β-Bi_2O_3 / $Bi_5O_7NO_3$ phases (see Table 1).

3.4. TG analysis

The TG and TA analyses of the as-prepared samples are shown in

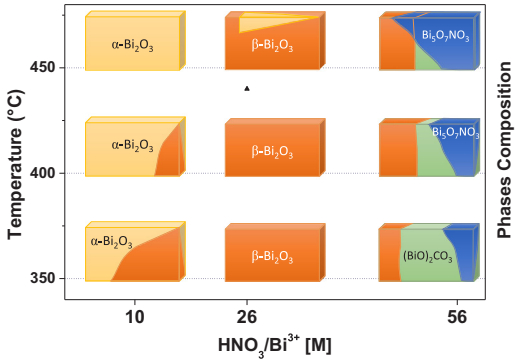

Fig. 4. Schematic diagram phase compositions of Bi_2O_3 as function of annealing temperature from different as-prepared precursor at molar ratio HNO_3/Bi^{3+} (10, 26 and 56).

Fig. 5A–B. For the amorphous **NB10** solid, the first weight loss (3.4%) at the temperature interval of 28–250 °C was associated with the exothermic peak at 234 °C, which could be related to the dehydration of either basic bismuth nitrate or $(BiO)_4CO_3(OH)_2$ compound by replacing OH^- by CO_3^{-2} ions [55]. After that, in the interval 250–419 °C, the weight loss corresponds to the thermal decomposition of carbonates [16], which is accompanied by two exothermic peaks at 335 and 396 °C. These events are related to the transformation of $(BiO)_2CO_3$ into the β-Bi_2O_3 and α-Bi_2O_3 phases [58], respectively, as observed by XRD (Fig. 1A).

As for the amorphous **NB26** solid, the first weight loss (3.4%) occurred at of 28–170 °C, corresponding to the elimination of physisorbed water. Then in the interval 170–240 °C, the exothermic peak at 210 °C is related to the dehydration of $(BiO)_4CO_3(OH)_2$ to form $(BiO)_2CO_3$ [53]. From 250 to 409 °C, two exothermic peaks at 290 and 313 °C are observed, corresponding to the thermal decomposition of carbonates and the ENH^+-molecule, respectively. The peak at 290 °C is also related to the transformation of $(BiO)_2CO_3$ to β-Bi_2O_3. In addition, a small exothermic peak at 510 °C is observed, which can be related to the crystallization of the α-Bi_2O_3 phase, as suggested by XRD (Fig. 1B). Thus, it can be seen that the β-Bi_2O_3 phase is stable at higher temperatures than in previous reports, where the transformation into α-Bi_2O_3 at around 320–350 °C has been observed [2,38,40,58].

For the nanocrystalline **NB56** solid, the first weight loss (3.4%) occurred at 28–184 °C, corresponding to the elimination of physisorbed water from $Bi_6O_6(OH)_2(NO_3)_4{\cdot}2H_2O$ compounds [59]. Then, in the interval 184–400 °C, two exothermic peaks at 244 and 352 °C are observed, which are related to the transformation of $(BiO)_2CO_3$ into β-Bi_2O_3 and to the release-decomposition of the NO_3^- group [60] to form $Bi_5O_7NO_3$ compounds, respectively. From 400 to 532 °C, the endothermic peak at 509 °C must be related to the decomposition of $Bi_5O_7NO_3$ and crystallization of the α-Bi_2O_3 phase [45,61].

3.5. SEM and textural properties of Bi_2O_3

The SEM images of all the amorphous precursors and the annealed solids containing the β-Bi_2O_3 phase are shown in Fig. 6A–C. The obtained amorphous **NB10** solid exhibited huge micro-sheet morphology with heterogeneous sizes (Fig. 6A), where their lengths (*L*) can reach 5–20 μm and the thickness (*th*) is ~ 0.1 μm. However, small nanoparticles can be seen deposited on top of the microsheets, which could be related to the presence of $(BiO)_2CO_3$. When annealed at 350 °C, the microsheets remained and irregular nanoparticles are also observed. The irregular nanoparticles can be related to the β-Bi_2O_3 phase while sheet-particles are associated with the α-Bi_2O_3 phase. This is more evident in the solids annealed at 400 and 450 °C (not shown), where the α-Bi_2O_3 phase is in high proportion (see Fig. 1).

The amorphous $(BiO)_4CO_3(OH)_2$ compounds (**NB26** solid) exhibited nanoparticles with leaflet morphology with dimensions of L = 0.5–1 μm and *th* = 10–50 nm (Fig. 6B). This morphology is typical of carbonate intermediate compounds [53], which exhibit the appearance of lamellar structure, which is in agreement with the diffracted peak at low angle in XRD (Fig. 1B). After the calcination at 350 °C, the β-Bi_2O_3 phase showed melt-like-leaflet morphology, until reaching irregular nanoparticles of 50–100 nm at 450 °C. Similar morphology has been reported for the β-Bi_2O_3 phase obtained from the $(BiO)_2CO_3$ precursor [1].

In the case of the basic bismuth nitrate **NB56** solid, rectangular sheet morphology was observed with dimensions of L = 10 μm, width of 2–3 μm and *th* = 100 nm (Fig. 6C), however, small leaflet-morphology nanoparticles were also observed, which could be attributed to the presence of the amorphous $(BiO)_2CO_3$ precursor. The morphology of basic bismuth nitrate in the lamellar structure is in good agreement with the literature [46]. When $Bi_6O_6(OH)_2(NO_3)_4{\cdot}2H_2O$ is transformed into $(BiO)_2CO_3$ /$Bi_5O_7NO_3$ at 400 °C, it exhibits smaller fractured sheets whereas the formed β-Bi_2O_3 phase also exhibited irregular nanoparticles similar to those obtained with the **NB10–350** sample.

Based on the SEM results, both the particle size and morphology strongly depend on the type and composition of the bismuth-based precursor, which also depends on the HNO_3/Bi^{3+} molar ratio, finding optimal contents to obtain irregular nanoparticles of the stabilized β-Bi_2O_3 phase.

Textural characterization was measurement for the solids containing β-Bi_2O_3 phase (NB10-350 and NB56–350) and for the well stabilized β-Bi_2O_3 phase at high temperature (NB26–450). These annealed solids exhibited an isotherm of N_2 adsorption-desorption (Fig. S1) categorized as type IV according to the IUPAC classification. Additionally, they exhibited a H3 hysteresis loop increasing in the order for NB10–350, NB26–450 and NB56–350 suggesting the presence of mesoporous structure, resulting from the inter-microsheets/

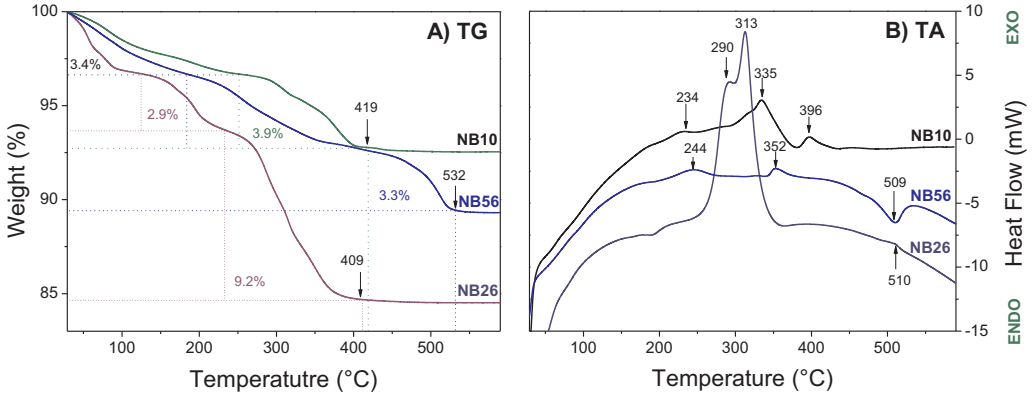

Fig. 5. A) TG and B) TA curves of the as-prepared samples at different molar ratio HNO_3/Bi^{3+} (10, 26 and 56).

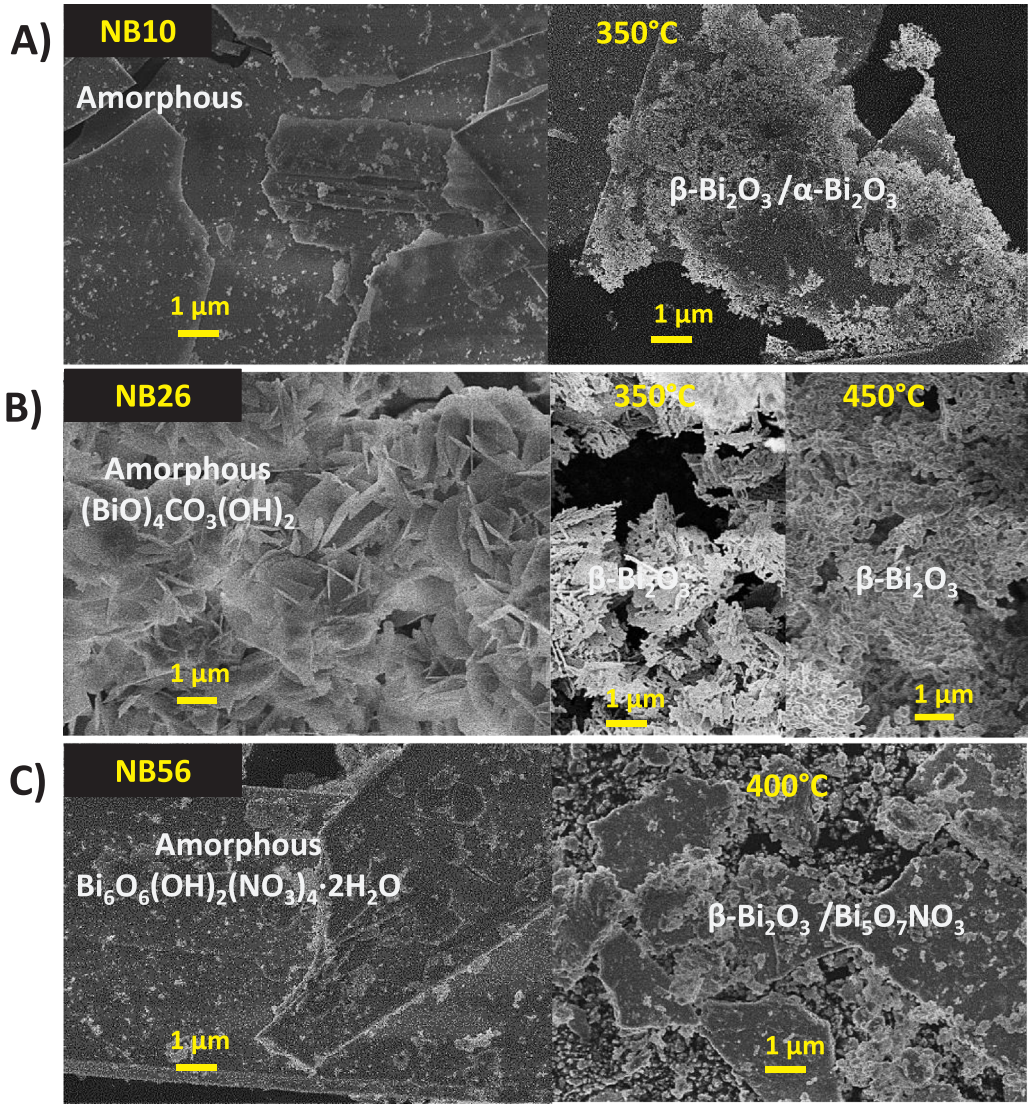

Fig. 6. SEM image of as-prepared prepared at different molar ratio HNO_3/Bi^{3+}: A) 10, B) 26 and C) 56 and its respective annealed solids.

microcrystals and fibrous structures [51]. The specific surface area for the well stabilized β-Bi_2O_3 phase is ~ 5 m^2/g. For the other solids containing mixture of phases, the specific surface area is in the same interval ~ 4–8 m^2/g (see Table 1), suggesting that it depends of the phase composition.

3.6. Optical properties

The UV–vis diffuse reflectance spectra (DRS) of all the solids are shown in Fig. 7A–C. As for the amorphous **NB10** solid (Fig. 7A), the absorbance edge starts at ~500 nm with a maximum absorption at ~ 260 nm, indicating absorption in the UV light region. Similar absorption at 350–500 nm has been observed for carbonate precursors, where surface defects occurred [51,62]. For the solid annealed at 350 °C, the absorption extends into the visible region at 390–550 nm, corresponding to the electronic transition from the valence band to the conduction band of the β-Bi_2O_3 phase [4]. But at 400 and 450 °C, the absorption is blue-shifted at 340–440 nm, which is characteristic to the electronic transition of the α-Bi_2O_3 phase [24]. According to the emission spectrum of the blue LED lamp (inset in Fig. 7A), the solid containing the β-Bi_2O_3 phase (**NB10–350)** can be activated by the blue-light absorption.

For the **NB26** solid (Fig. 7B), the absorbance edge starts at ~ 360 nm with a maximum absorption at ~ 270 nm, indicating absorption in the UV light region, which is characteristic of the electronic transition of $(BiO)_4CO_3(OH)_2$ compounds [53]. After the calcination at 350–450 °C, all solids present absorption from ~ 550 to ~ 380 nm, which is characteristic of electronic transitions of the pure β-Bi_2O_3 phase [16]. The β-Bi_2O_3 phase can be fully activated by the blue light emitted by the LED lamp (inset in Fig. 7B).

In the case of the **NB56** solid (Fig. 7C), the absorbance edge observed at ~ 310–400 nm corresponds to the electronic transition of basic bismuth nitrate ($Bi_6O_6(OH)_2(NO_3)_4{\cdot}2H_2O$) [44], also indicating absorption in the UV light region. When annealed at 350 °C, the absorption edge extends toward the visible range from 400 to 550 nm. This visible absorption is due to the presence of both the β-Bi_2O_3 and $Bi_5O_7NO_3$ phases that are present in higher proportion at high annealing temperatures.

The band gap energies of all the solids were determined by using the Kubelka-Munk function considering the type of fundamental transitions, direct or indirect, as indicated in Table 1. The absorption in the visible light region is very important for photocatalytic applications, therefore, the annealed solids containing the β-Bi_2O_3 phase with band gap within the 2.4 ± 0.04 eV interval [2,31] were used for the photocatalytic test under blue light.

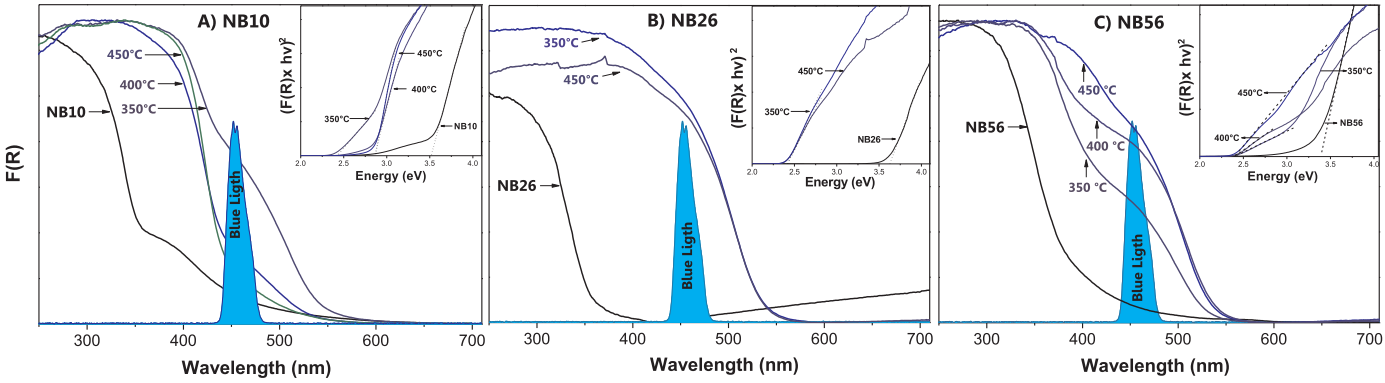

Fig. 7. UV–vis DRS spectra the as-prepared samples at molar ratio HNO_3/Bi^{3+}; A) 10, B) 26 and C) 56, and of the annealed solids from 350 to 450 °C. Optical band gap estimation ban gap energy is inset.

3.7. Blue-Photocatalytic activity and mechanism

The dye adsorption capacity and photocatalytic activity in the photodegradation of Indigo Carmine (*IC*) dye displayed by the solids containing the β-Bi_2O_3 phase were evaluated under dark conditions and blue irradiation, respectively. The absorbance spectrum of the *IC* dye solution exhibited the typical absorbance peak at 610 nm, characteristic of the *indigoid group* [63]. The decrease in this peak almost negligible for 40 min of adsorption, but it was drastically decreased after 50 min of blue irradiation using the **NB26–350** solid (Fig. 8). This fast decrease in the *indigoid* absorbance is accompanied by the increase in the already known isosbestic point at 251 nm and the raised absorbance peak at 218 nm, which suggests that the *IC* dye was degraded to isatin sulfonic and 2-amino-5-sulfobenzoic acids [64,65]. Both intermediates are products of the oxidation reaction by the superoxide radical (•O_2-) [66].

Fig. 9A shows the relative concentration profile (C/C_0) of the *IC* dye during the adsorption and blue degradation time using the **NB10-, NB26-** and **NB56–350** solids. The adsorption capacity of the pure β-Bi_2O_3 solid is very low, reaching only 3% of adsorbed IC dye whereas for the solid containing α/β-Bi_2O_3 (**NB10-350**), the dye adsorption is 9%. During the blue-degradation time, the C/C_0 of the *IC* dye decreased with the reaction time, reaching a maximum of 85% of *IC* dye degradation in 50 min using the pure β- Bi_2O_3 solid (**NB26–350**). By plotting $\ln(C_0/C)$ versus the reaction time (t), a straight line is obtained, which is characteristic of a pseudo first order reaction (1st order, not shown). From this plot, the apparent kinetic rate constant (K_{app}) of all the annealed solids was estimated and the values are shown in Fig. 9B. All the solids with low content of the β-Bi_2O_3 phase presented a lower $K_{app} < 1.0 \times 10^{-2}$ min^{-1}; on the other hand, for the pure β-Bi_2O_3 solids, their K_{app} are close to $3.5 \pm 0.2 \times 10^{-2}$ min^{-1}. Despite of the low specific surface area (~ 4–8 m^2/g) of the solids, the pure stabilized β-Bi_2O_3 phase showed high photocatalytic activity under blue light, probably because it has better charge separation efficiency than the α/β-Bi_2O_3 mixture or the mixture of the $(BiO)_2CO_3$ / β-Bi_2O_3 / $Bi_5O_7NO_3$ phases because on the one hand, their blue absorption is limited and on the other hand, the charge separation does not occur.

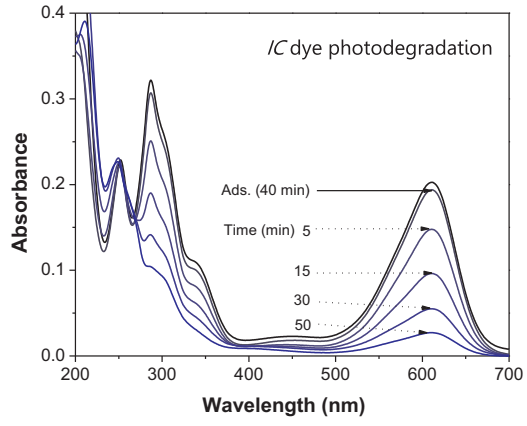

Fig. 8. Absorbance spectra of *IC* dye solution during dark condition and blue light irradiation, using **NB26–350** solid.

The mass variation study using stabilized pure β- Bi_2O_3 (**NB26–450,** not shown), revealed that 0.1 g/L of solid is the optimum load for the photocatalytic *IC* dye degradation. In this case, the load is very low in comparison to other reported studies [34,35], which is probably due to the nanometric size of the pure β-Bi_2O_3 solid.

Considering that the blue energy provide by the Blue-LED lamp is not sufficiently powerful to induce the photolysis of water for the generation of OH• radicals [67], it means that the blue-photogenerated electrons on β-Bi_2O_3 solid can be captured by dissolved O_2 to generate superoxide (•O_2^-) radicals. The conduction band of the β-Bi_2O_3 solid at the natural pH of the IC dye solution (pH ~7) must be more negative than that of the couple $O_2/•O_2^-$ (-0.13 V) [68], and as a consequence large amounts of •O_2^- radicals are formed, which are responsible for the oxidation of the IC dye. The efficiency for the generation of these superoxide radicals is well achieved despite that the stabilized β-Bi_2O_3 solid was annealed at high temperature.

4. Conclusion

Pure β-Bi_2O_3 solids, well-stabilized at temperatures ranging from 350 to 450 °C and with excellent photocatalytic response to the visible-light degradation of indigo carmine dye solutions, can be obtained by annealing amorphous $(BiO)_4CO_3(OH)_2$ compounds, which were prepared by chemical precipitation using an optimal HNO_3/Bi^{3+} molar ratio equal to 26 in the presence of ethylenediamine solvent. The amorphous product prepared with a HNO_3/Bi^{3+} molar ratio equal to 10 led to the α/β-Bi_2O_3 mixture at 350–400 °C with subsequent transformations to α-Bi_2O_3 at 400 °C whereas a high HNO_3/Bi^{3+} molar ratio equal to 56 favors the formation of basic bismuth nitrate, which is the precursor of the mixture of $(BiO)_2CO_3$/β-Bi_2O_3/$Bi_5O_7NO_3$ phases. The synthesis of either pure Bi_2O_3 or a mixture of the bismuth-based compounds depends strongly on the amount of CO_3^{2-} and NO_3^-, and amine (ENH_2^{2+} ⇔ENH^+) ions present in the bismuth precursor, which also depends on the molar ratio of HNO_3/Bi^{3+} ions in the presence of an ethylenediamine aqueous solution.

Acknowledgments

The author wants to thank CONACYT for the Catedras-Conacyt/1169 support. The authors also acknowledge the financial support from the CONACYT 251276 project. Finally, the authors acknowledge the support provided by A. Tejeda, M.A. Canseco, Eriseth Morales, V.

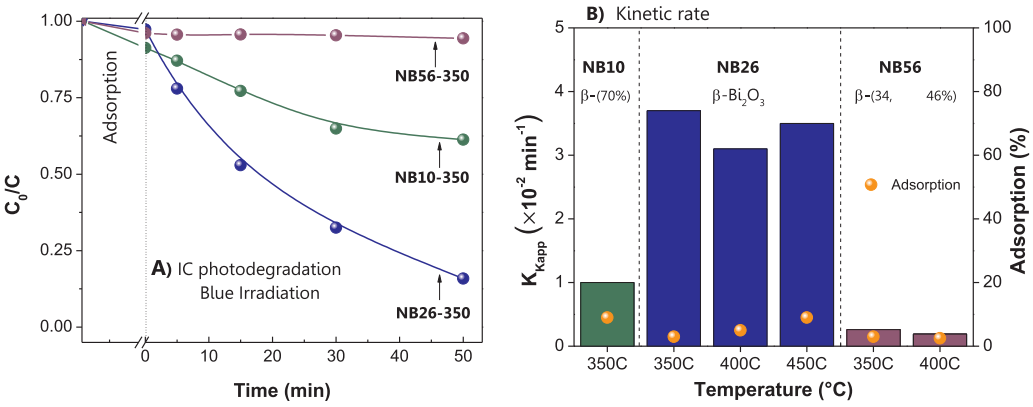

Fig. 9. A) Profile of relative concentration and B) Apparent kinetic rate of the *IC* dye photodegradation of the evaluated solids.

Maturano, Lazaro Huerta and O. Novelo for making possible different measurements.

Appendix A. Supplementary material

Supplementary data associated with this article can be found in the online version at doi:10.1016/j.ceramint.2018.08.358.

References

[1] H.-Y. Jiang, P. Li, G. liu, J. Ye, J. Lin, Synthesis and photocatalytic properties of metastable β-Bi2O3 stabilized by surface-coordination effects, J. Mater. Chem. A 3 (2015) 5119–5125.

[2] Y. Yan, Z. Zhou, Y. Cheng, L. Qiu, C. Gao, J. Zhou, Template-free fabrication of α- and β-Bi2O3 hollow spheres and their visible light photocatalytic activity for water purification, J. Alloy. Compd. 605 (2014) 102–108.

[3] M. Vila, C. Díaz-Guerra, K. Lorenz, J. Piqueras, E. Alves, S. Nappini, E. Magnano, Structural and luminescence properties of Eu and Er implanted Bi2O3 nanowires for optoelectronic applications, J. Mater. Chem. C 1 (2013) 7920.

[4] N.M. Khusayfan, A.F. Qasrawi, H.K. Khanfar, Impact of Yb, In, Ag and Au thin film substrates on the crystalline nature, Schottky barrier formation and microwave trapping properties of Bi 2 O 3 films, Mater. Sci. Semicond. Process. 64 (2017) 63–70.

[5] X.-J. Ma, W.-B. Zhang, L.-B. Kong, Y.-C. Luo, L. Kang, β-Bi 2 O 3: an underlying negative electrode material obeyed electrode potential over electrochemical energy storage device, Electrochim. Acta 192 (2016) 45–51.

[6] A. Cabot, A. Marsal, J. Arbiol, J.R. Morante, Bi2O3 as a selective sensing material for NO detection, Sens. Actuators B: Chem. 99 (2004) 74–89.

[7] T. Lu, Z. Du, J. Liu, H. Ma, J. Xu, Aerobic oxidation of primary aliphatic alcohols over bismuth oxide supported platinum catalysts in water, Green Chem. 15 (2013) 2215.

[8] S. Gong, Q. Han, X. Wang, J. Zhu, Controlled synthesis of bismuth-containing compounds (α-, β- and δ-Bi2O3, Bi5O7NO3 and Bi6O6(OH)2(NO3)4·2H2O) and their photocatalytic performance, CrystEngComm 17 (2015) 9185–9192.

[9] M. Schlesinger, M. Weber, S. Schulze, M. Hietschold, M. Mehring, Metastable beta-Bi2O3 nanoparticles with potential for photocatalytic water purification using visible light irradiation, ChemistryOpen 2 (2013) 146–155.

[10] R. He, D. Xu, B. Cheng, J. Yu, W. Ho, Review on nanoscale Bi-based photocatalysts, Nanoscale Horiz. 3 (2018) 464–504.

[11] R. He, J. Zhou, H. Fu, S. Zhang, C. Jiang, Room-temperature in situ fabrication of Bi 2 O 3 /g-C 3 N 4 direct Z-scheme photocatalyst with enhanced photocatalytic activity, Appl. Surf. Sci. 430 (2018) 273–282.

[12] W. He, Y. Sun, G. Jiang, H. Huang, X. Zhang, F. Dong, Activation of amorphous Bi 2 WO 6 with synchronous Bi metal and Bi 2 O 3 coupling: photocatalysis mechanism and reaction pathway, Appl. Catal. B: Environ. 232 (2018) 340–347.

[13] A. Hezam, K. Namratha, Q.A. Drmosh, Z.H. Yamani, K. Byrappa, Synthesis of heterostructured Bi 2 O 3 –CeO 2 –ZnO photocatalyst with enhanced sunlight photocatalytic activity, Ceram. Int. 43 (2017) 5292–5301.

[14] Z. Liang, Y. Cao, Y. Li, J. Xie, N. Guo, D. Jia, Solid-state chemical synthesis of rod-like fluorine-doped β-Bi 2 O 3 and their enhanced photocatalytic property under visible light, Appl. Surf. Sci. 390 (2016) 78–85.

[15] D. Xu, Y. Hai, X. Zhang, S. Zhang, R. He, Bi 2 O 3 cocatalyst improving photocatalytic hydrogen evolution performance of TiO 2, Appl. Surf. Sci. 400 (2017) 530–536.

[16] G. Cai, L. Xu, B. Wei, J. Che, H. Gao, W. Sun, Facile synthesis of β-Bi2O3/Bi2O2CO3 nanocomposite with high visible-light photocatalytic activity, Mater. Lett. 120 (2014) 1–4.

[17] Y. Bian, Y. Ma, Y. Shang, P. Tan, J. Pan, Self-integrated β-Bi 2 O 3 /Bi 2 O 2.33 @Bi 2 O 2 CO 3 ternary composites: formation mechanism and visible light photocatalytic activity, Appl. Surf. Sci. 430 (2018) 613–624.

[18] Y. Shi, L. Luo, Y. Zhang, Y. Chen, S. Wang, L. Li, Y. Long, F. Jiang, Synthesis and characterization of α/β-Bi 2 O 3 with enhanced photocatalytic activity for 17α-ethynylestradiol, Ceram. Int. 43 (2017) 7627–7635.

[19] C. Wu, L. Shen, Q. Huang, Y.-C. Zhang, Hydrothermal synthesis and characterization of Bi2O3 nanowires, Mater. Lett. 65 (2011) 1134–1136.

[20] S. Iyyapushpam, S.T. Nishanthi, D. Pathinettam Padiyan, Photocatalytic degradation of methyl orange using α-Bi2O3 prepared without surfactant, J. Alloy. Compd. 563 (2013) 104–107.

[21] Y. Wu, G. Lu, The roles of density-tunable surface oxygen vacancy over bouquet-like Bi2O3 in enhancing photocatalytic activity, physical chemistry chemical physics, PCCP 16 (2014) 4165–4175.

[22] G. Guenther, O. Guillon, Solid state transitions of Bi2O3 nanoparticles, J. Mater. Res. 29 (2014) 1383–1392.

[23] H. Oudghiri-Hassani, S. Rakass, F.T. Al Wadaani, K.J. Al-ghamdi, A. Omer, M. Messali, M. Abboudi, Synthesis, characterization and photocatalytic activity of α-Bi2O3 nanoparticles, J. Taibah Univ. Sci. 9 (2015) 508–512.

[24] S. Sood, A. Umar, S. Kumar Mehta, S. Kumar Kansal, α-Bi2O3 nanorods: an efficient sunlight active photocatalyst for degradation of Rhodamine B and 2,4,6-trichlorophenol, Ceram. Int. 41 (2015) 3355–3364.

[25] A.M. Abu-Dief, W.S. Mohamed, α-Bi2O3nanorods: synthesis, characterization and UV-photocatalytic activity, Mater. Res. Express 4 (2017) 035039.

[26] Y. Lu, Y. Zhao, J. Zhao, Y. Song, Z. Huang, F. Gao, N. Li, Y. Li, Photoactive β-Bi2O3 architectures prepared by a simple solution crystallization method, Ceram. Int. 40 (2014) 15057–15063.

[27] X. Xiao, R. Hu, C. Liu, C. Xing, C. Qian, X. Zuo, J. Nan, L. Wang, Facile large-scale synthesis of β-Bi2O3 nanospheres as a highly efficient photocatalyst for the degradation of acetaminophen under visible light irradiation, Appl. Catal. B: Environ. 140–141 (2013) 433–443.

[28] X. Xiao, S. Tu, C. Zheng, H. Zhong, X. Zuo, J. Nan, L-Asparagine-assisted synthesis of flower-like β-Bi2O3 and its photocatalytic performance for the degradation of 4-phenylphenol under visible-light irradiation, RSC Adv. 5 (2015) 74977–74985.

[29] J. Wang, X. Yang, K. Zhao, P. Xu, L. Zong, R. Yu, D. Wang, J. Deng, J. Chen, X. Xing, Precursor-induced fabrication of β-Bi2O3 microspheres and their performance as visible-light-driven photocatalysts, J. Mater. Chem. A 1 (2013) 9069.

[30] K. Barrera-Mota, M. Bizarro, M. Castellino, A. Tagliaferro, A. Hernandez, S.E. Rodil, Spray deposited beta-Bi2O3 nanostructured films with visible photocatalytic activity for solar water treatment, Photochem. Photobiol. Sci.: Off. J. Eur. Photochem. Assoc. Eur. Soc. Photobiol. 14 (2015) 1110–1119.

[31] Y. Qiu, M. Yang, H. Fan, Y. Zuo, Y. Shao, Y. Xu, X. Yang, S. Yang, Nanowires of α- and β-Bi2O3: phase-selective synthesis and application in photocatalysis, CrystEngComm 13 (2011) 1843–1850.

[32] H. Cheng, B. Huang, J. Lu, Z. Wang, B. Xu, X. Qin, X. Zhang, Y. Dai, Synergistic effect of crystal and electronic structures on the visible-light-driven photocatalytic performances of Bi(2)O(3) polymorphs, Phys. Chem. Chem. Phys.: PCCP 12 (2010) 15468–15475.

[33] G. Zhu, Y. Liu, M. Hojamberdiev, J. Han, J. Rodríguez, S.A. Bilmes, P. Liu, Thermodecomposition synthesis of porous β-Bi2O3/Bi2O2CO3 heterostructured photocatalysts with improved visible light photocatalytic activity, New J. Chem. 39 (2015) 9557–9568.

[34] A. Charanpahari, S.S. Umare, R. Sasikala, Enhanced photodegradation of dyes on Bi2O3 microflakes: effect of GeO2 addition on photocatalytic activity, Sep. Purif. Technol. 133 (2014) 438–442.

[35] Y. Wang, Y. Wen, H. Ding, Y. Shan, Improved structural stability of titanium-doped β-Bi2O3 during visible-light-activated photocatalytic processes, J. Mater. Sci. 45 (2009) 1385–1392.

[36] L. Liu, J. Jiang, S. Jin, Z. Xia, M. Tang, Hydrothermal synthesis of β-bismuth oxide nanowires from particles, CrystEngComm 13 (2011) 2529.

[37] R. Chen, Z.-R. Shen, H. Wang, H.-J. Zhou, Y.-P. Liu, D.-T. Ding, T.-H. Chen, Fabrication of mesh-like bismuth oxide single crystalline nanoflakes and their visible light photocatalytic activity, J. Alloy. Compd. 509 (2011) 2588–2596.

[38] R. Hu, X. Xiao, S. Tu, X. Zuo, J. Nan, Synthesis of flower-like heterostructured β-Bi2O3/Bi2O2CO3 microspheres using Bi2O2CO3 self-sacrifice precursor and its visible-light-induced photocatalytic degradation of o-phenylphenol, Appl. Catal. B: Environ. 163 (2015) 510–519.

[39] Z. Zhang, D. Jiang, C. Xing, L. Chen, M. Chen, M. He, Novel AgI-decorated beta-Bi (2)O(3) nanosheet heterostructured Z-scheme photocatalysts for efficient degradation of organic pollutants with enhanced performance, Dalton Trans. 44 (2015) 11582–11591.
[40] R. Moré, M. Olah, S.E. Balaghi, P. Jäker, S. Siol, Y. Zhou, G.R. Patzke, Bi2O2CO3 growth at room temperature: in situ X-ray diffraction monitoring and thermal behavior, ACS Omega 2 (2017) 8213–8221.
[41] L. Shan, Y. Liu, H. Chen, Z. Wu, Z. Han, An alpha-Bi2O3/BiOBr core-shell heterojunction with high photocatalytic activity, Dalton Trans. 46 (2017) 2310–2321.
[42] H.B. Yao, M.R. Gao, S.H. Yu, Small organic molecule templating synthesis of organic-inorganic hybrid materials: their nanostructures and properties, Nanoscale 2 (2010) 323–334.
[43] J. Pang, Q. Han, W. Liu, Z. Shen, X. Wang, J. Zhu, Two basic bismuth nitrates: [Bi 6 O 6 (OH) 2](NO 3) 4·2H 2 O with superior photodegradation activity for rhodamine B and [Bi 6 O 5 (OH) 3](NO 3) 5·3H 2 O with ultrahigh adsorption capacity for methyl orange, Appl. Surf. Sci. 422 (2017) 283–294.
[44] L.-M. Yang, G.-Y. Zhang, Y. Liu, Y.-Y. Xu, C.-M. Liu, J.-W. Liu, A {110} facet predominated Bi6O6(OH)3(NO3)3·1.5H2O photocatalyst: selective hydrothermal synthesis and its superior photocatalytic activity for degradation of phenol, RSC Adv. 5 (2015) 79715–79723.
[45] A.H.A. Eshraq Ahmed Abdullah, Zulkarnain Zainal, Mohd Zobir Hussein, Tan Kar Ban, Synthesis and characterisation of penta-bismuth hepta-oxide nitrate, Bi5O7NO3, as a new adsorbent for methyl orange removal from an aqueous solution, Eur.-J. Chem. 9 (4) (2012) 2429–2438.
[46] A.H.A.E.A. Abdullah, Z. Zainal, M.Z. Hussein, T.K. Ban, Bismuth basic nitrate as a novel adsorbent for azo dye removal, Eur.-J. Chem. 9 (4) (2012) 1885–1896.
[47] M.-A.C. Axel Nørlund Christensen, Jørgen Skibsted, Bo B. Iverse, Synthesis and characterization of basic bismuth(III) nitrates, J. Chem. Soc. Dalton Trans. (2000) 265–270.
[48] A. Hernandez-Gordillo, S. Oros-Ruiz, R. Gomez, Preparation of efficient cadmium sulfide nanofibers for hydrogen production using ethylenediamine (NH2CH2CH2NH2) as template, J. Colloid Interface Sci. 451 (2015) 40–45.
[49] J.Z. Marinho, L.M. Santos, L.R. Macario, E. Longo, A.E.H. Machado, A.O.T. Patrocinio, R.C. Lima, Rapid preparation of (BiO)2CO3 nanosheets by microwave-assisted hydrothermal method with promising photocatalytic activity under UV–vis light, J. Braz. Chem. Soc. (2015).
[50] F. Dong, Y. Sun, W.K. Ho, Z. Wu, Controlled synthesis, growth mechanism and highly efficient solar photocatalysis of nitrogen-doped bismuth subcarbonate hierarchical nanosheets architectures, Dalton Trans. 41 (2012) 8270–8284.
[51] W. Cen, T. Xiong, C. Tang, S. Yuan, F. Dong, Effects of morphology and crystallinity on the photocatalytic activity of (bio)2CO3 nano/microstructures, Ind. Eng. Chem. Res. 53 (2014) 15002–15011.
[52] L. Huang, G. Li, T. Yan, J. Zheng, L. Li, Uncovering the structural stabilities of the functional bismuth containing oxides: a case study of α-Bi2O3nanoparticles in aqueous solutions, New J. Chem. 35 (2011) 197–203.
[53] F. Dong, T. Xiong, R. Wang, Y. Sun, Y. Jiang, Growth mechanism and photocatalytic activity of self-organized N-doped (BiO)(2)CO(3) hierarchical nanosheet microspheres from bismuth citrate and urea, Dalton Trans. 43 (2014) 6631–6642.
[54] F. Dong, A. Zheng, Y. Sun, M. Fu, B. Jiang, W.-K. Ho, S.C. Lee, Z. Wu, One-pot template-free synthesis, growth mechanism and enhanced photocatalytic activity of monodisperse (BiO)2CO3 hierarchical hollow microspheres self-assembled with single-crystalline nanosheets, CrystEngComm 14 (2012) 3534.
[55] F. Dong, W.-K. Ho, S.C. Lee, Z. Wu, M. Fu, S. Zou, Y. Huang, Template-free fabrication and growth mechanism of uniform (BiO)2CO3 hierarchical hollow microspheres with outstanding photocatalytic activities under both UV and visible light irradiation, J. Mater. Chem. 21 (2011) 12428.
[56] K. Uchida, A. Ayame, Dynamic XPS measurements on bismuth molybdate surfaces, Surf. Sci. 357–358 (1996) 170–175.
[57] G.-H. Hwang, W.-K. Han, J.-S. Park, S.-G. Kang, An electrochemical sensor based on the reduction of screen-printed bismuth oxide for the determination of trace lead and cadmium, Sens. Actuators B: Chem. 135 (2008) 309–316.
[58] Z. Ai, Y. Huang, S. Lee, L. Zhang, Monoclinic α-Bi2O3 photocatalyst for efficient removal of gaseous NO and HCHO under visible light irradiation, J. Alloy. Compd. 509 (2011) 2044–2049.
[59] F. Lazarini, Thermal dehydration of some basic bismuth nitrates, Thermochim. Acta 46 (1981) 53–55.
[60] H. Kodama, Synthesis on new compound, Bi5O7NO3 by thermal decomposition, J. Solid State Chem. 112 (1994) 27–30.
[61] N. Henry, O. Mentré, F. Abraham, E.J. MacLean, P. Roussel, Polycationic disorder in [Bi6O4(OH)4](NO3)6: structure determination using synchrotron radiation and microcrystal X-ray diffraction, J. Solid State Chem. 179 (2006) 3087–3094.
[62] J. Tang, H. Zhao, G. Li, Z. Lu, S. Xiao, R. Chen, Citrate/urea/solvent mediated Self-assembly of (BiO)2CO3 hierarchical nanostructures and their associated photocatalytic performance, Ind. Eng. Chem. Res. 52 (2013) 12604–12612.
[63] Y. Kohno, S. Kitamura, T. Yamada, K. Sugihara, S. Ohta, Production of superoxide radical in reductive metabolism of a synthetic food-coloring agent, indigocarmine, and related compounds, Life Sci. 77 (2005) 601–614.
[64] M.G. Coelho, G.M. de Lima, R. Augusti, D.A. Maria, J.D. Ardisson, New materials for photocatalytic degradation of indigo carmine—synthesis, characterization and catalytic experiments of nanometric tin dioxide-based composites, Appl. Catal. B: Environ. 96 (2010) 67–71.
[65] C.M. Antonio-Cisneros, M.M. Davila-Jimenez, M.P. Elizalde-Gonzalez, E. Garcia-Diaz, TiO2 immobilized on Manihot carbon: optimal preparation and evaluation of its activity in the decomposition of indigo carmine, Int. J. Mol. Sci. 16 (2015) 1590–1612.
[66] A.J. Kettle, B.M. Clark, C.C. Winterbourn, Superoxide converts indigo carmine to isatin sulfonic acid: implications for the hypothesis that neutrophils produce ozone, J. Biol. Chem. 279 (2004) 18521–18525.
[67] Y. Sun, W. Wang, L. Zhang, S. Sun, The photocatalysis of Bi2MoO6 under the irradiation of blue LED, Mater. Res. Bull. 48 (2013) 4357–4361.
[68] J.C. Medina, N.S. Portillo-Vélez, M. Bizarro, A. Hernández-Gordillo, S.E. Rodil, Synergistic effect of supported ZnO/Bi 2 O 3 heterojunctions for photocatalysis under visible light, Dyes Pigments 153 (2018) 106–116.